JCTC Journal of Chemical Theory and Computation

7-Norbornyl Cation − Fact or Fiction? A QTAIM-DI-VISAB Computational Study

Nick H. Werstiuk*

Department of Chemistry, McMaster University, Hamilton ON L8S 4M1, Canada

Received July 15, 2007

Abstract: QTAIM-DI-VISAB analyses were used to characterize the bonding of the 'nonclassical' 7-norbornyl cation and its rearrangement transitions states. These analyses involved obtaining QTAIM molecular graphs and delocalization indexes (DIs) that were correlated with the proximities of atomic basins (VISAB). This study showed that the so-called 7-norbornyl cation actually exhibits the molecular graph of the bicyclo[3.2.0]heptyl cation at its equilibrium geometry. Dynamical aspects of its molecular graph/density were explored with QTAIM by analyzing the nuclear motions of the 206 cm^{-1} normal mode. This study cements the QTAIM-DI-VISAB analysis as a method of choice for establishing the nature of the bonding in so-called nonclassical carbocations while obviating the need for dotted-line representations of bonding.

Introduction

The structure of the 7-norbornyl cation (**1**) was the focus of many experimental and theoretical studies for several decades, one of the latest being the work of Mesić et al.[1] This activity followed the suggestion by Winstein[2] in 1958 that it should be considered as a tricycloheptonium nonclassical cation shown in its usual dashed-line representation as **7-like**; this cation was considered as the common intermediate generated in solution by solvolysis of 7-bicyclo[2.2.1]heptyl *p*-bromobenzenesulfonate and exo-2-bicyclo[3.2.0]heptyl *p*-bromobenzenesulfonate.[2−4] The hypothetical 2-bicyclo[3.2.0]heptyl cation is shown as **2**. The first standard high-level computational study on the so-called 7-norbornyl cation was carried out by Sieber et al.[5] in 1993, and it recently has been implicated in reaction mechanisms of the fragmentation of 7-norbornyloxy(chloro)carbene.[6] In all publications to this point the species in question has been named the 7-norbornyl cation, and a variety of dashed-line structural formulas was used, including the usual ones that are 7-norbornyl-like—shown as **7-like**—and 2-bicyclo[3.2.0]-like shown as **[3.2.0]-like**.

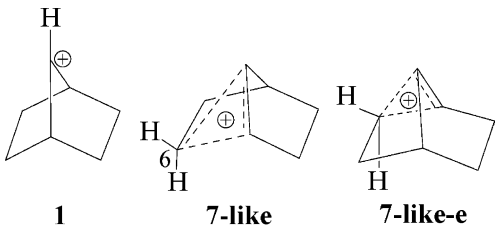

In fact, dotted/dashed lines, hollow tubes, and solid tubes of ORTEP drawings, and combinations thereof have been used in publications in attempts to represent the bonding of this so-called nonclassical carbocation with the implication being that C6 of **7-like** is a pentacoordinate atom. In exploring the 7-norbornyl potential energy surface computationally, Sieber et al.[5] located three species

* Corresponding author phone: (905)525-9140; fax: (905)522-2509; e-mail: werstiuk@mcmaster.ca.

10.1021/ct700176d CCC: $37.00
Published on Web 10/24/2007

as stationary points—**1-*C*$_1$**, **1-*C*$_S$**

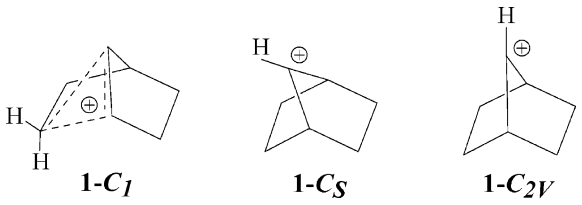

1-*C*$_1$ **1-*C*$_S$** **1-*C*$_{2V}$**

in which C7 leaned toward one ethano bridge, and **1-*C*$_{2V}$** at the MP2(full)/6-31G(d) level. However, **1-*C*$_S$** and **1-*C*$_{2V}$** possessed an imaginary frequency; based on the nature of the vibrational mode corresponding to the imaginary frequency, **1-*C*$_S$** was viewed as the transition state for the same-face degenerate rearrangement of **1-*C*$_1$** to its enantiomer **7-like-e**, and **1-*C*$_{2V}$** the transition state for bridge flapping of **1-*C*$_S$**; the details of the potential energy surface for the **1-*C*$_1$**, **1-*C*$_S$**, and **1-*C*$_{2V}$** interconversion were not defined.

Our recent computational studies on a number of cations, including 2-norbornyl, established that coordination based on the number of bond paths—as defined in a QTAIM (Quantum Theory of Atoms in Molecules)[7] molecular graph—terminating at a nucleus in any species—cation, carbanion, radical, or carbene—should be used as the criterion of hypercoordination and hypervalency.[8−11] We argued that this approach should be used regardless of the nature of the intermediate to obviate the confusion and inaccuracies associated with using indicators such as dashed lines, dotted lines, cross-hatched lines, hollow tubes, and solid tubes in structural formulas. In addition to using QTAIM molecular graphs to show *molecular* structure we recently showed that QTAIM-DI-VISAB analyses—a combination of QTAIM molecular graphs, an evaluation of delocalization indexes (DIs), and a visualization of the closeness of atomic basins (VISAB)—are useful for characterizing the bonding in molecules at their equilibrium geometries.[12,13] This paper reports the results of a QTAIM-DI-VISAB study on the bonding of the so-called 7-norbornyl cation.

Computational Methods

Our previous experiences with DFT calculations on carbocations clearly showed that the B3PW91 hybrid functional is superior to B3LYP in computing the geometries of delocalized, so-called nonclassical species.[8−11] To provide additional support for this finding, calculations were carried out on O-protonated 2,2-dimethyloxirane—studied recently by Carlier et al.[14] and described as a particularly challenging computational problem—to compare results from B3LYP, B3PW91, PBE1PBE, and CCSD calculations at the 6-311G(d,p) level as implemented in G03.[15] The results—including Carlier's data obtained at the 6-311++G(d,p) level shown in italics—are summarized in Figure 1. It is clear that B3PW91 and PBE1PBE are expected to be superior to B3LYP in cases where relatively weak polar bonds are involved. Cation geometries were optimized at B3PW91/6-311G(d,p), PEB1PBE/6-311G(d,p), and CCSD(full)/6-311G(d,p) levels with GaussView[16] being used to fix C_S and C_{2V} symmetries where necessary. Selected internuclear distances are collected in Figure 2, and the Cartesian

Method	C-O(Å)
CCSD	*1.599*
MP2	*1.598*
PBE1PBE	*1.634*
B3PW91	*1.671*
B3LYP	*1.790*
CCSD/6-311G(d,p)	1.593
PBE1PBE/6-311G(d,p)	1.628
B3PW91/6-311G(d,p)	1.660
B3LYP/6-311G(d,p)	1.731

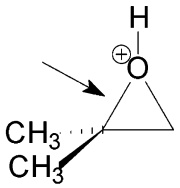

Figure 1. C−O distances of O-protonated 2,2-dimethyloxirane at various levels of theory. Data in italics obtained by Carlier et al. at 6-311++G(d,p).

coordinates of the optimized geometries are given in Tables 1S−9S (Supporting Information). The average geometry—Cartesian coordinates are given in Table 10S (Supporting Information)—of **1-*C*$_1$** at 0 K was obtained with a G03 FREQ=ANHARM calculation at B3PW91/6-311G(d,p). Cation **1-*C*$_1$** was also studied at the B3PW91 and PBE1PBE levels with the Carlier basis set (6-311++G(d,p)) to probe the effect of increasing basis-set size; the results—values in brackets—given in Figure 2 show that the geometrical effects are negligible. Frequency calculations were carried out on the stationary points at the 6-311G(d,p) level to confirm them as energy minima or transitions states. CCSD minima were confirmed with MP2 frequency calculations. Thermochemical data are collected in Table 1 (B3PW91), Table 2 (PBE1PBE), and Table 3 (CCSD). While $\Delta E^{\ddagger}_{\mathrm{lec}}$, $\Delta E^{\ddagger}_{0}$, $\Delta E^{\ddagger}_{298}$, and $\Delta H^{\ddagger}_{298}$ were computed, only $\Delta E^{\ddagger}_{\mathrm{elec}}$, $\Delta H^{\ddagger}_{298}$, ΔE_{elec}, and ΔH_{298} are included in the discussion.

QTAIM analyses of the wave functions to investigate the topologies of the electron densities were carried out with AIM2000,[17] and values of $\rho(\mathbf{r}_c)$ at selected bond critical points are collected in Figure 3. AIMALL97[18] was used to integrate atomic basins, to obtain atomic populations, total charges, and atomic overlap matrices required for DI calculations. That the total charges of **1-*C*$_1$**, **1-*C*$_S$**, and **1-*C*$_{2V}$** obtained at the various levels of theory (Figure 3) were less than 1% higher than the expected value of 1.0 onfirmed the quality and validity of the QTAIM data. The program LI-DICALC[19,20] was used to obtain DIs; selected values for pairs of atoms are listed in Figure 4. Isosurface plots of the density (Figure 5(b),(c)) and the Laplacian of the density (Figure 5(d)) were obtained with the B3PW91/6-311G(d,p) wave function using NABLA[21] to obtain the grid points and OpenDX[22] to generate the plots. Atomic basins were obtained with AIM2000 at a contour value of 0.005 au—this includes >95% of the electrons—using a mesh grid size of 0.125 and plotted with a sphere size of 0.15. GaussView[16] was used to simulate an IR spectrum of **1-*C*$_1$** and obtain nuclear displacement vectors. GaussView and ChemCraft[23] were used to animate the normal modes; the 206 cm^{-1} mode, the one that appeared to bring C2 and C7 within a distance where a BP could be formed, was selected for a detailed analysis. Using ChemCraft, the nuclear motions of this mode—the G03 displacement coordinates were scaled by 0.35—were frozen

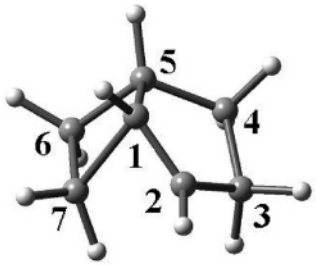

1-C_1

	B3PW91	PBE1PBE	CCSD
C1-C2	1.388[1.388]	1.387[1.387]	1.388
C2-C3	1.497	1.499	1.515
C4-C5	1.537	1.533	1.540
C5-C6	1.542	1.539	1.544
C6-C7	1.547	1.546	1.557
C1-C7	1.751[1.751]	1.747[1.748]	1.797
C1-C5	1.535[1.535]	1.531[1.531]	1.535
C2-C7	1.955[1.954]	1.908[1.909]	1.899

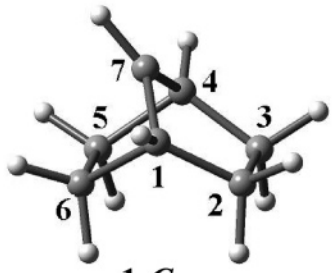

1-C_S

	B3PW91	PBE1PBE	CCSD
C1-C2	1.536	1.533	1.541
C2-C3	1.559	1.555	1.564
C5-C6	1.585	1.583	1.587
C1-C6	1.547	1.591	1.596
C1-C7	1.447	1.445	1.456
C2-C7	2.379	2.375	2.385
C6-C7	2.044	2.030	2.080

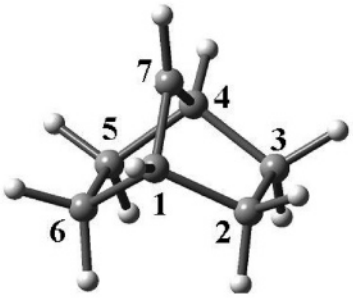

1-C_{2V}

	B3PW91	PBE1PBE	CCSD
C1-C2	1.566	1.562	1.566
C2-C3	1.565	1.562	1.569
C2-C6	2.531	2.523	2.528
C1-C7	1.456	1.455	1.489
C2-C7	2.282	2.277	2.294

Figure 2. Selected internuclear distances of **1-C_1**, **1-C_S**, and **1-C_{2V}** at B3PW91, PBE1PBE, and CCSD(full). Values in square brackets obtained with the Carlier basis set (6-311++G(d,p)).

Table 1. Total and Relative Energies of Cations at B3PW91/6-311G(d,p)

				protonated alcohols	
cation	**1-C_1**	**1-C_S**	**1-C_{2V}**	**3**	**4**
E_{elec}[a]	−273.009458 (*0.00*)	−273.003910 (*3.48*)[e] (−233.4 cm^{-1})[g]	−272.998026 (*7.17*)[e] (−321.2 cm^{-1})[g]	−349.473743 (*0.00*)	−349.455802 (*11.26*)[f]
E_0[b]	−272.846302 (*0.00*)	−272.841025 (*3.32*)	−272.835234 (*6.65*)	−349.280161 (*0.00*)	−349.264575 (*9.78*)
E_{298}[c]	−272.840116 (*0.00*)	−272.835415 (*2.95*)	−272.829529 (*6.64*)	−349.272751 (*0.00*)	−349.256556 (*10.16*)
H_{298}[d]	−272.839172 (*0.00*)	−272.834471 (*2.95*)	−272.828585 (*6.64*)	−349.271806 (*0.00*)	−349.255612 (*10.16*)

[a] E_{elec} is the uncorrected total energy in hartrees. [b] $E_0 = E_{elec}$ + ZPE. [c] $E = E_0 + E_{vib} + E_{rot} + E_{trans}$. [d] $H = E + RT$. [e] Values in brackets relative to **1-C_1** in kcal mol^{-1}. [f] Relative to 3. [g] The imaginary frequency.

Table 2. Total and Relative Energies of Cations at PBE1PBE/6-311G(d,p)

cation	**1-C_1**	**1-C_S**	**1-C_{2V}**
E_{elec}[a]	−272.774310(*0.00*)	−272.768946(*3.36*)[e] (−244.4 cm^{-1})[f]	−272.762413(*7.74*)[e] (−330.3 cm^{-1})[f]
E_0[b]	−272.610299(*0.00*)	−272.605325(*2.79*)	−272.598889(*7.16*)
E_{298}[c]	−272.604191(*0.00*)	−272.599745(*2.79*)	−272.593200(*6.90*)
H_{298}[d]	−272.603247(*0.00*)	−272.598801(*2.79*)	−272.592256(*6.90*)

[a] E_{elec} is the uncorrected total energy in hartrees. [b] $E_0 = E_{elec}$ + ZPE. [c] $E = E_0 + E_{vib} + E_{rot} + E_{trans}$. [d] $H = E + RT$. [e] Values in brackets relative to **1-C_1** in kcal mol^{-1}. [f] The imaginary frequency.

at ten intervals including geometries with the largest (2.118) and shortest distances (1.795 Å) between C2 and C7. Cartesian-coordinate files were written, and single-point calculations with SCF=TIGHT were carried out to obtain wave functions. The C2−C7 distances, uncorrected electronic energies (E_{elec}), and relative energies (ΔE_{elec}) of the ten geometries along with the equilibrium geometry of **1-C_1** are collected in Table 4. QTAIM analyses of the wave functions

Table 3. Total and Relative Energies of Cations at CCSD(full)/6-311G(d,p) and MP2(full)/6-311G(d,p)

cation	**1-C_1**	**1-C_S**	**1-C_{2V}**
CCSD(full)/6-311G(d,p)			
E_{elec}[a]	−272.440844 (0.00)	−272.436078 (+2.99)[f]	−272.431628 (+5.78)[f]
MP2(full)/6-311G(d,p)[b]			
E_{elec}[b]	−272.371813(0.00)	−272.363435 (5.26)	−272.356284 (9.74)
		(−315.0)[g]	(−322.6)[g]
E_0[b,c]	−272.206471 (0.00)	−272.198947 (4.72)	−272.191814 (9.19)
E_{298}[b,d]	−272.200445 (0.00)	−272.193318 (4.47)	−272.186104 (9.00)
H_{298}[b,e]	−272.199501 (0.00)	−272.192372 (4.47)	−272.185160 (9.00)

[a] E_{elec} is the uncorrected CCSD(full) total energy in hartrees. [b] From a single point frequency calculation at MP2(full)/6-311G(d,p) on the CCSD(full)/6-311G(d,p) geometry. [c] $E_0 = E_{elec} + ZPE$. [d] $E = E_0 + E_{vib} + E_{rot} + E_{trans}$. [e] $H = E + RT$. [f] Values in brackets relative to **1-C_1** in kcal mol^{-1}. [g] The imaginary frequency.

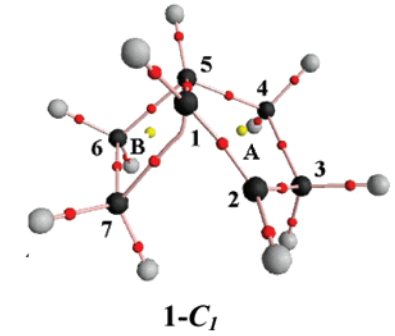

1-C_1

	B3PW91	PBE1PBE	CCSD
C1-C2	0.3132	0.3133	0.3122
C2-C3	0.2560	0.2555	0.2500
C3-C4	0.2320	0.2341	0.2334
C4-C5	0.2393	0.2416	0.2412
C5-C6	0.2382	0.2403	0.2408
C6-C7	0.2323	0.2380	0.2312
C1-C7	0.1390	0.1413	0.1361
C1-C5	0.2415	0.2437	0.2439
RCP A	0.0431	0.0439	0.0419
RCP B	0.0783	0.0796	0.0743
Charge	+1.0039	+1.0048	+1.0013

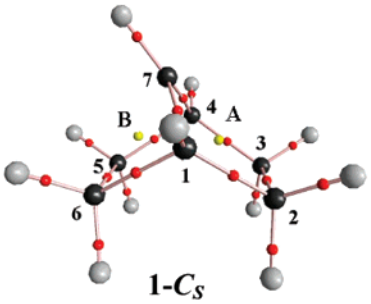

1-C_S

	B3PW91	PBE1PBE	CCSD
C1-C2	0.2381	0.2401	0.2388
C2-C3	0.2288	0.2306	0.2299
C5-C6	0.2183	0.2194	0.2212
C1-C6	0.2035	0.2062	0.2077
C1-C7	0.2821	0.2830	0.2789
RCP A	0.0438	0.0444	0.0424
RCP B	0.0656	0.0678	0.0606
Charge	+1.0024	+1.0026	+1.0027

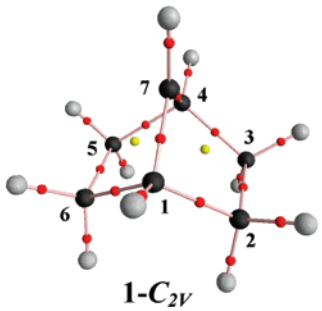

1-C_{2V}

	B3PW91	PBE1PBE	CCSD
C1-C2	0.2193	0.2218	0.2231
C2-C3	0.2275	0.2294	0.2289
C1-C7	0.2804	0.2811	0.2756
RCP	0.0477	0.0486	0.0461
Charge	+1.0036	+1.0062	+1.0010

Figure 3. QTAIM molecular graphs of **1-C_1**, **1-C_S**, and **1-C_{2V}** at B3PW91, values of $\rho(\mathbf{r})$ at bond and ring critical points of **1-C_1**, **1-C_S**, and **1-C_{2V}**, and total charges at B3PW91, PBE1PBE, and CCSD(full): black spheres carbons, gray spheres hydrogens, red spheres BCPs, and yellow spheres RCPs.

yielded 11 molecular graphs that were converted to JPEG files—the molecular graphs along with frame numbers are displayed in Figure 4S (Supporting Information). The JPEG files were combined in the sequence (also see Table 4 for assignments) F1, F2, F3, F4, F5, F6, F7, F8, F9, F8, F7, F6, F5, F4, F3,F2, F1, F10, F11, F10, and F1 to yield a 21-frame animation of the changes in the bicyclo[3.2.0]heptyl molecular graph during the nuclear motions associated with the 206 cm^{-1} mode. The resulting motion picture—viewable with common media players such as Windows Media Player—is included in the Supporting Information.

Results and Discussion

Thermochemistry. At all levels of theory **1-C_1** is a minimum on the PE surface, and **1-C_S** and **1-C_{2V}** are transition states. Based on the normal mode associated with its imaginary frequency, **1-C_S** is the transition state for the same-face rearrangement of **1-C_1** to its enantiomer. The barrier of this

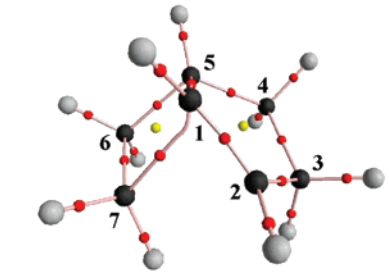

1-C_1

	B3PW91	PBE1PBE	CCSD
C1-C2	1.2558	1.2517	1.0741
C4-C5	0.9649	0.9662	0.8139
C5-C6	0.9519	0.9533	0.8020
C6-C7	0.9511	0.9505	0.7953
C1-C7	0.6150	0.6069	0.4527
C1-C5	0.9346	0.9353	0.7895
C2-C7	0.4287	0.4570	0.3783

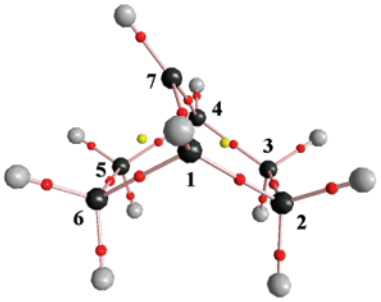

1-C_S

	B3PW91	PBE1PBE	CCSD
C1-C2	0.9590	0.9609	0.8080
C2-C3	0.9607	0.9622	0.8045
C1-C6	0.8513	0.8545	0.7243
C1-C7	1.0684	1.0665	0.9017
C2-C7	0.0621	0.0620	0.0483
C6-C7	0.2289	0.2328	0.1572
C2-C6	0.0422	0.0428	0.0321

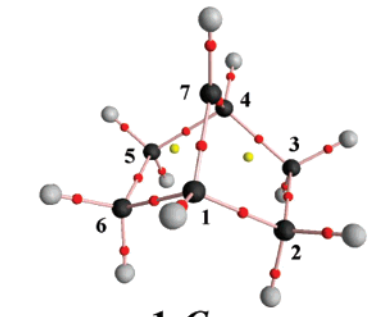

1-C_{2V}

	B3PW91	PBE1PBE	CCSD
C1-C2	0.9019	0.9046	0.7683
C1-C7	1.0689	1.0657	0.8956
C2-C7	0.1224	0.1221	0.0851
C2-C6	0.0446	0.0451	0.0336

Figure 4. QTAIM molecular graphs of **1-C_1**, **1-C_S**, and **1-C_{2V}** at B3PW91 and delocalization indices of selected atom pairs of **1-C_1**, **1-C_S**, and **1-C_{2V}** at B3PW91, PBE1PBE, and CCSD(full).

degenerate rearrangement is very low—$\Delta H^{\ddagger}_{298}$ is in the range of 3 kcal mol^{-1} at B3PW91 (Table 1), PBE1PBE (Table 2), and CCSD(full) (Table 3) levels. There is little variation in going from $\Delta E(\Delta E^{\ddagger})$ to $\Delta H_{298}(\Delta H^{\ddagger}_{298})$. **1-$C_{2V}$** is higher in energy than **1-C_S**—the values of $\Delta H^{\ddagger}_{298}$ for the bridge flapping from **1-C_S** at the three levels of theory are 3.69 (B3PW91), 4.11 (PBE1PBE), and 4.53 (CCSD(full)/MP2(full)) kcal mol^{-1}. **1-C_{2V}** exhibits only one large negative eigenvalue and, as indicated by the nature of the 'vibrational mode' associated with the imaginary frequency, **1-C_{2V}** appears to be the transition state for bridge flapping between **1-C_S** ions ($\Delta H_{298} = \Delta H^{\ddagger}_{298}$). This result suggests that the '7-norbornyl cation' gas-phase PE surface is characterized by a bifurcation pathway as displayed in Figure 4(b) of a paper by Xantheas et al.[24] The values of $\Delta H^{\ddagger}_{298}$ relative to **1-C_1** are 6.64 (B3PW91), 6.90 (PBE1PBE), and 9.00 (CCSD/MP2) kcal mol^{-1}. O-protonated 7-norbornanol (**3**) and O-protonated exo-2-bicyclo[3.2.0]heptanol (**4**) were also studied at the B3PW91/6-311G(d,p) level. The molecular graphs of **3** and **4** are displayed in parts (a) and (b), respectively, of Figure 1S along with internuclear distances and values of $\rho(\mathbf{r}_c)$—in parentheses—of selected BCPs (Supporting Information). At this level, **3** is significantly lower in energy than **4**; ΔH_{298} is −10.16 kcal mol^{-1}. This result is in keeping with the fact that 7-norbornyl substituted products predominate in the solvolysis of 7-norbornyl and 2-bicyclo[3.2.0]heptyl substrates.[2−4]

Equilibrium Molecular and Geometrical Structures. *1-C_1*. The molecular graph of the equilibrium geometry of the '7-norbornyl' cation obtained at the B3PW91/6-311G(d,p) level is displayed in Figure 3 (**1**-C_1), Figure 4 (**1**-C_1), and Figure 5(a). It is clear that the so-called 7-norbornyl cation, in fact, exhibits the bicyclo[3.2.0]heptyl cation molecular graph at its equilibrium geometry! Identical molecular graphs (not displayed) were also obtained at the PBE1PBE/6-311G(d,p), CCSD(full)/6-311G(d,p), B3PW91/6-311++G(d,p), and PBE1PBE/6-311++G(d,p) levels. The plots of the density ($\rho(\mathbf{r})$) of the equilibrium geometry at contour values of 0.095 (Figure 5(b)) and 0.125 au (Figure 5(c)) and the Laplacian ($-\nabla^2\rho$) (Figure 5(d), contour value 0.005) are nicely in accord with the [3.2.0] molecular graph. Neither shows a 'bridge' that includes C2 and C7. The key point is that C7 does not have five bond paths terminating at the nucleus. Consequently, **1-C_1** is NOT a pentacoordinate

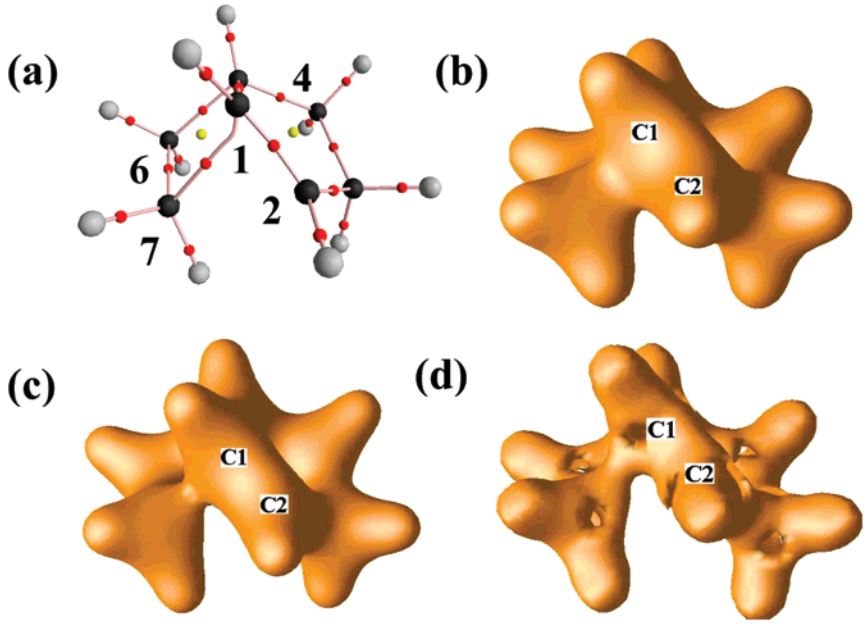

Figure 5. (a) Molecular graph of **1-*C*$_1$** at B3PW91/6-311G(d,p); (b) density (ρ) of **1-*C*$_1$** at a contour value of 0.095; (c) density (ρ) of 1-***C*$_1$** at a contour value of 0.125; and (d) Laplacian ($-\nabla^2\rho$) of **1-*C*$_1$** at a contour value of 0.005 at B3PW91/6-311G(d,p).

Table 4. Total and Relative Energies of Freeze-Frame Geometries of the 206 cm^{-1} Mode of **1-*C*$_1$** at B3PW91/6-311G(d,p)

C2−C7 distance/Å[a]	E_{elec}[b]	ΔE_{elec}/kcal mol^{-1} (relative to the equilibrium geometry)
2.118(max.)[**F11**][c]	−273.008135	0.830
1.994[**F10**]	−273.009382	0.048
1.954(equil geom)[**F1**]	−273.009458	0.000
1.906[**F2**]	−273.009338	0.075
1.858[**F3**]	−273.008939	0.326
1.821[**F4**]	−273.008412	0.656
1.816[**F5**]	−273.008327	0.710
1.814[**F6**]	−273.008291	0.733
1.812[**F7**]	−273.008256	0.754
1.807[**F8**]	−273.008142	0.826
1.795(min.)[**F9**]	−273.007949	0.947

[a] Freeze-frame analysis carried out with ChemCraft: the G03 206 cm^{-1} mode; displacement coordinates scaled by 0.35. [b] The uncorrected total energy E_{elec} in hartrees. [c] The frame numbers of the molecular graphs used in the molecular-graph motion picture. See Figure 3S (Supporting Information).

species in its equilibrium geometry. This is also the case at the PBE1PBE and CCSD levels—the CCSD molecular graph is displayed as Figure 2S(a) (Supporting Information)—even though the C2−C7 internuclear distances are significantly shorter in these cases relative to the B3PW91. At all levels, C1−C2 exhibits considerable double-bond character. The internuclear distances are all close to 1.39 Å, and the $\rho(r_c)$ values at the BCPs lie in the region of 0.31 au, considerably higher than the values (Figure 3) of 0.24 and 0.22 for the C1−C2 BCPs of **1-*C*$_S$** and **1-*C*$_{2V}$**, respectively. C1−C7 of **1-*C*$_1$** is a weak bond—$\rho(\mathbf{r}_c)$ lies in the region of 0.13 to 0.14—relative to C1−C6 of **1-*C*$_S$** (0.2035) and **1-*C*$_{2V}$** (0.2193).

That vibrational frequencies were calculated prompted an examination of the normal modes of **1-*C*$_1$**. In nuclear configuration space there may be an arrangement of nuclei where C2 and C7 are transiently connected by a BP due to molecular vibrations. This may be general in cases of this type where the density is flat and there is a high ellipticity of bonds with the soft axis laying in the 3-atom plane along the existing BPs. This appears to be the case in **1-*C*$_1$**; the ellipticity is 1.790 at the C1−C7 BCP, significantly higher than the ellipticity (0.011) at BCP of the 'normal' single bond C4−C5 of **1-*C*$_1$**. The simulated IR spectrum of **1-*C*$_1$** computed with G03 exhibited two strong bands at 206 and 536 cm^{-1}. When animated, only the 206 cm^{-1} mode of the bands below 600 cm^{-1} appeared to bring C2 and C7 closer together, possibly to a point where a BP and BCP transiently materialize between C2 and C7. To establish whether the nuclear motions of the 206 cm^{-1} mode resulted in the formation of a BCP/BP between C2 and C7, ChemCraft was used to freeze the nuclear motions—the G03 displacement coordinates were scaled by 0.35—at ten intervals to obtain snapshots of displacement geometries. The C2−C7 distances ranged from 2.118 to 1.795 Å (Table 4). It is seen that the C1−C7 BP switches to a highly curved BP between C2 and C7 when the C2−C7 distance was 1.814 Å (**F6**, Figure 4S (Supporting Information)) with the 1.814-Å geometry being 0.733 kcal mol^{-1} higher in energy than the equilibrium geometry. Given that the 206 cm^{-1} mode has a ZPE of 0.295 kcal mol^{-1} ((206 cm^{-1} × 2.86 cal cm^{-1})/2) it is unlikely that the 1.814-Å geometry is achieved at 0 K. Moreover, the average geometry of **1-*C*$_1$** at 0 K does not exhibit a BP between C2 and C7 (molecular graph not shown). The 1.816-Å geometry also exhibits a molecular graph that closely approaches a T-structure (**F5**, Figure 4S) we found for the equilibrium geometry of the 2-norbornyl cation.[10] It is important to note that Pendas et al.[25] have confirmed that QTAIM BCPs/BPs are valid probes of bonding in nonequilibrium structures. The point is that **1-*C*$_1$** exhibits a bicyclo-[3.2.0] molecular graph at its equilibrium geometry, and it does not exhibit a pentacoordinate C7 as it does not have

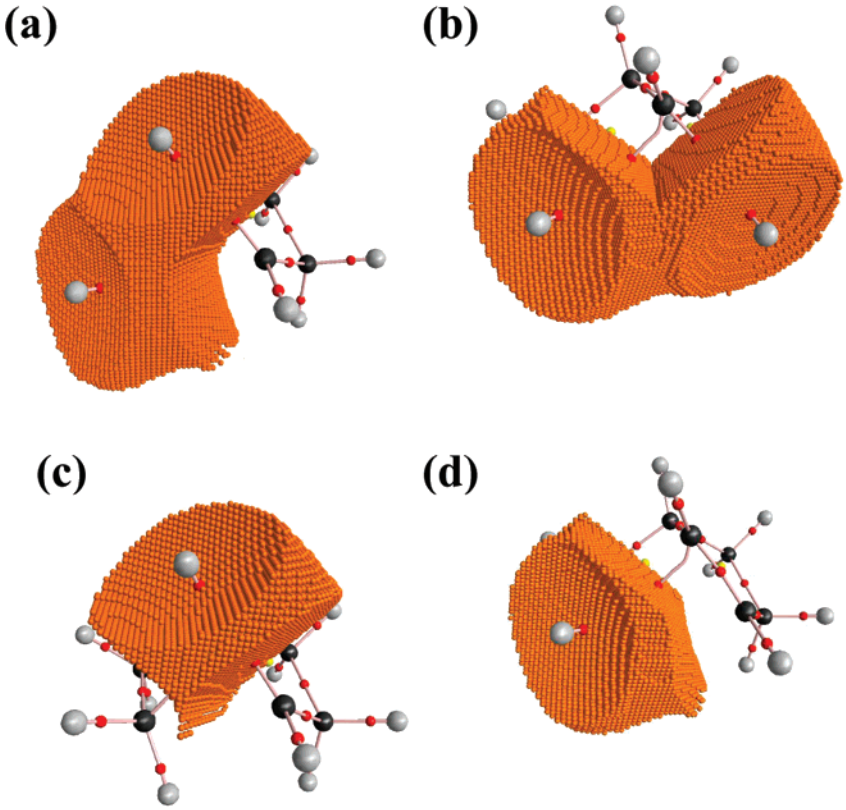

Figure 6. Atomic basins of **1-*C*$_1$** at B3PW91/6-311G(d,p): (a) C1, C7; (b) C2, C7; (c) C1; and (d) C7.

five bond paths terminating at the nucleus even during the 206 cm^{-1} vibration.

***1-C*$_S$**. The molecular graph of **1-*C*$_S$** obtained at the B3PW91/6-311G(d,p) level is displayed in Figures 3 (**1-*C*$_S$**) and 7(a). Identical molecular graphs (not displayed) were obtained at the PBE1PBE/6-311G(d,p) and CCSD(full)/6-311G(d,p) levels as well. Even though C7 leans toward C5 and C6—the C7−C5(C7−C6) distance is 0.335 Å less than the C7−C2(C7−C3) distance—there is no bond path between C7 and C5 or C7 and C6. This was also the case even at PBE1PBE where the C7−C6(C7−C5) distance was 0.014 Å less than at the B3PW91 level. It is seen that the C5−C6 bond, toward which C7 leans, is longer (+0.026, +0.027, and +0.022 Å at B3PW91, PBE1PBE, and CCSD) and slightly weaker than the C2−C3 bond. This is supported by the fact that the $\rho(\mathbf{r}_c)$ values at the BCPs at B3PW91 are 0.2183 and 0.2387, respectively. C1−C7and C4−C7 exhibit double-bond character; the internuclear distances are 1.447 Å, and the $\rho(\mathbf{r}_c)$ values at the BCPs are 0.2821, 0.2830, and 0.2780 at the B3PW91, PBE1PBE, and CCSD levels, respectively. Based on the $\rho(\mathbf{r})$ values at the RCPs (0.0438 for ring A and 0.0656 for ring B), the bridge lean results in an increase in the density in ring B.

***1-C*$_{2V}$**. The molecular graph of **1-*C*$_{2V}$** obtained at the B3PW91/6-311G(d,p) level is displayed as Figure 3 (**1-*C*$_{2V}$**) and as Figure 8(a). Identical molecular graphs (not displayed) were obtained at the B3PW91/6-311G(d,p) and CCSD/6-311G(d,p) levels as well. There are no bond paths between C7 and C2, C3, C5, and C6 at any level. It is seen that C1−C2 and C3−C4 bonds are shortened relative to the C1−C2 and C3−C4 bonds of **1-*C*$_S$** (0.0188 Å), and C4−C5, C6−C1 bonds are lengthened (0.0158 Å) relative to C4−C5, C6−C1 of **1-*C*$_S$**. The C2−C3 bond is marginally shorter than the C2−C3 bond of **1-*C*$_S$**, and C5−C6 is marginally longer than C5−C6 of **1-*C*$_S$**. The values of $\rho(r_c)$ at the BCPs at the B3PW91 are 0.2183 and 0.2387.

O-Protonated Alcohols 3 and 4. The molecular graphs of O-protonated 7-norbornanol (**3**) and exo-2-bicyclo[3.2.0]-heptanol (**4**) along with selected internuclear distances and values of $\rho(\mathbf{r}_c)$ at the BCPs are displayed in Figure 1S. Protonation of the alcohols leads to a significant lengthening if the C−O bonds and several C−C bonds; the C−O distances of the parent alcohols 7-norbornanol and exo-2-bicyclo[3.2.0]heptanol are 1.410 and 1.426 Å, respectively. In terms of the internuclear distance and the value of $\rho(\mathbf{r}_c)$ at the BCP, the C−O bond of **4** is weaker than the C−O bond of **3**.

QTAIM-DI-VISAB Analyses. *1-C*$_1$. Selected atomic basins of **1-*C*$_1$** obtained at the B3PW91 level are displayed as Figures 6(a−d) and 2S(a−c). Figure 6(a) shows the C1 and C7 basins of the C1−C7 bond. That these basins share an atomic surface is clearly seen in this display. The DI is 0.6150, substantially lower than the DI (0.9519) of the 'normal' C5−C6 single bond across the ring; C1−C7 is a relatively weak covalent bond. Figure 6(b) shows the C2 and C7 basins that are in very close proximity to each other. From a visual standpoint these basins are similar to the pair of carbon atoms of the C1−C7 bond, yet no bond path connects them even though the DI (0.4287) is relatively large. The reason for this result is readily seen in the display of the C1 basin shown as Figure 6(c); a 'wedge' of density of this basin intervenes between the C2 and C7 basins and

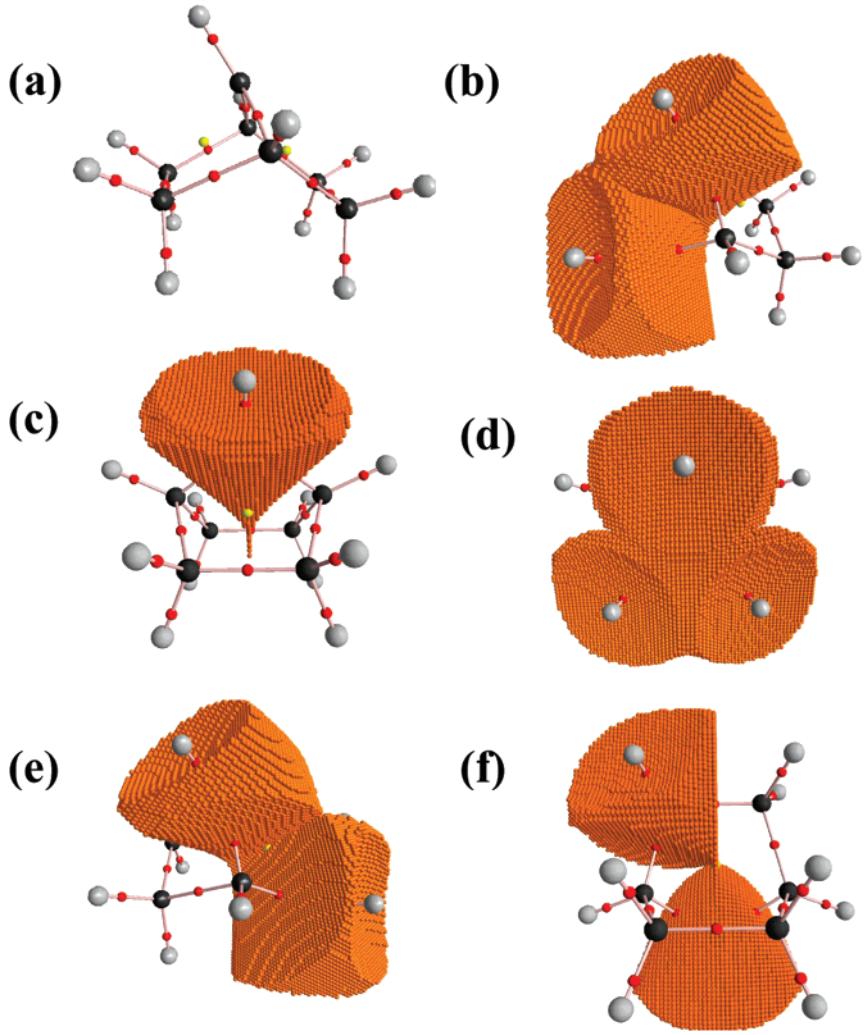

Figure 7. Molecular graph (a) and selected atomic basins of **1-*C*$_S$** at B3PW91/6- 311G(d,p): (b) C5, C7; (c) C7; (d) C5, C6, C7; (e) C2, C7; and (f) C2, C7 bottom view.

clearly precludes bond path formation. *Nevertheless there is a high degree of delocalization of electrons—the DI is 0.4287—between these basins in the absence of a bond path.* The flattening of the C7 atomic basin surface facing C2 is clearly seen in its display in Figure 6(d).

We observed this behavior—relatively large DIs but no BPs—previously in a number of cations[8−10] and in trimethylsilyl(carbene) and trimethylgermyl(carbene).[13] Farrugia et al. very recently observed this behavior in the case of the iron trimethylenemethane complex Fe(η^4-C{CH_3}$_3$)-$(CO)_3$ in an elegant high-resolution X-ray diffraction study that was coupled with B3LYP and QTAIM calculations.[26]

As a comparison, Figure 4S(a) shows the C4 and C6 basins on the other side of **1-*C*$_1$** that are not close to each other and exhibit a miniscule DI of 0.0455. It is interesting to note that there appears to be a weak interaction between $H7_{endo}$ and C2 as suggested by the proximity of these basins (Figure 4S(b)). The $H7_{endo}$ basin (Figure 4S(c)) shows some deformation, and the DI (0.0516) is nonzero. In keeping with our earlier results,[19,20] the CCSD DIs are somewhat lower than the DFT DIs. The molecular graph as well as the C7−C1, C7, C2, and C1 basins of **1-*C*$_1$** obtained at the CCSD(full)/6-311G(d,p) level (not shown) mirror the results obtained at B3PW91/6-311G(d,p).

***1-C*$_S$.** The molecular graph and selected atomic basins of **1-*C*$_S$** obtained at the B3PW91 level are displayed as Figure 7(a)−(f). While there are no bond paths between C5, C6, and C7, there is a significant exchange of electrons between the basins with the DI being 0.2289 for each pair—at the CCSD level the value is 0.1565—in keeping with their proximity. Figure 7(b) shows the C6 and C7 basins, 7(c) shows C7, and 7(d) shows the 3-basin cluster of C5, C6, and C7. This exchange/delocalization of electrons between C5, C6, and C7 is undoubtedly one of the reasons for the pronounced lean of C7 toward C5 and C6. The DI for the C2(C3), C7 pair is much smaller (0.0621) in keeping with the fact that they are farther apart than the C5(C6), C7 pairs as seen in Figure 7(e) and a bottom view in Figure 7(f). In keeping with the values of $\rho(\mathbf{r}_c)$ for the DI of the C1−C6 and C4−C5 bonds is smaller (0.8513) than the DI (0.9590) of C1−C2 and C3−C4 pairs indicating that the C1−C6 and C4−C5 bonds are weaker than the C1−C6 and C4−C5 bonds. The molecular graph as well as selected atomic basins of **1-*C*$_S$** obtained at the CCSD(full) level (not shown) mirror the results obtained at B3PW91/6-311G(d,p).

***1-C*$_{2V}$.** The molecular graph of **1-*C*$_{2V}$** and selected atomic basins obtained at the B3PW91 level are displayed as Figure 8(a)−(d). Figure 8(b) shows the C2 and C7 basins, 8(c)

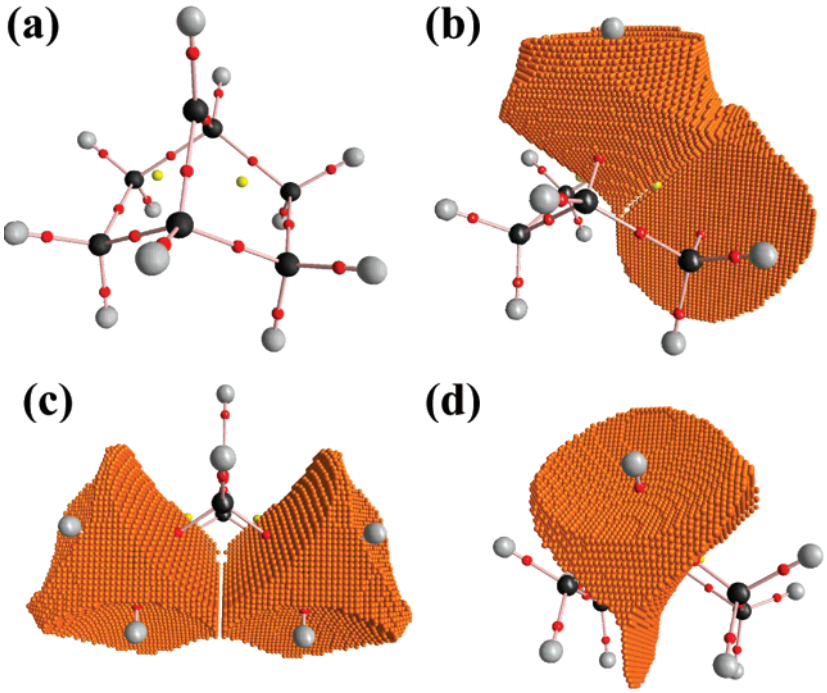

Figure 8. Molecular graph (a) and selected atomic basins of **1-*C*$_{2V}$** at B3PW91/6-311G(d,p): (b) C3, C7; (c) C2, C7; and (d) C1.

shows C6 and C2, and 8(d) shows the C1 basin. The C2 and C7 basins—this is also the case for the C3−C7, C5−C7, and C6−C7 pairs—do not have large proximate surface areas in keeping with the fact that the DI is 0.1224. While the DI is somewhat lower at the CCSD level (0.0849), these results clearly show that there is delocalization of electrons, although to a minor degree, between C7 and the ring carbons C2, C3, C5, and C6, contrary to the conclusions reached by Sunko et al.[27] on the basis of a simple molecular orbital analysis. Figure 8(c) is a display of the C2 and C6 basins that like the C2 and C7 basins do not have large proximate surfaces, and the DI (0.0446 at B3PW91 and 0.0334 at CCSD) is smaller than the DI for the C2−C7 pair. Figure 8(d) shows the C1 basin with the 'wedge' of density intervening between C2 and C6. In keeping with the relative values of $\rho(\mathbf{r}_c)$ (see Figure 3) the DI of C1−C2 (also C3−C4, C4−C5, and C1−C6) is smaller (0.9019) than the DI (0.9590) of the C1−C2(C3−C4) pairs of **1-*C*$_S$** indicating that these four ring C−C bonds are weaker than the C1−C2(C3−C4) bonds of **1-*C*$_S$**. However, in keeping with the relative values of $\rho(\mathbf{r}_c)$ (see Figure 3) the DI of C1−C2 (also C3−C4, C4−C5, and C1−C6) is larger (0.9019) than the DI (0.8513) of the C1−C6(C4−C5) pairs of **1-*C*$_S$** indicating that these four ring C−C bonds are stronger than the C1−C6(C4−C5) bonds of **1-*C*$_S$**. The molecular graph of **1-*C*$_{2V}$** and selected atomic basins obtained at the CCSD(full) level (not displayed) closely resemble the ones obtained at B3PW91.

Conclusions

This study shows that the so-called 7-norbornyl cation exhibits the molecular graph of the bicyclo[3.2.0]heptyl cation at its equilibrium geometry. It suggests that the QTAIM-DI-VISAB analysis is the method of choice for establishing the nature of the bonding in hypercoordinated so-called nonclassical carbocations. This approach obviates the need for dotted-line representations of bonding.

Acknowledgment. Financial support by the Natural Sciences and Engineering Research Council of Canada (NSERC) is gratefully acknowledged. Computing resources of the McMaster node of SHARCnet (Shared Hierarchical Academic Research Computing Network (of Ontario)) were used in this study.

Supporting Information Available: Cartesian coordinates of structures, selected figures, and a 21-frame animation (viewable with common media players such as Windows Media Player) of the changes in the bicyclo[3.2.0]-heptyl molecular graph during the nuclear motions associated with the 206 cm^{-1} mode. This material is available free of charge via the Internet at http://pubs.acs.org.

References

(1) Mesić, M. M.; Sunko, D. E.; Vančik, H. *J. Chem. Soc., Perkin Trans.* **1994**, *2*, 11.

(2) Winstein, S.; Gadient, F.; Stafford, E. T.; Klinedinst, P. E. *J. Am. Chem. Soc.* **1958**, *80*, 5895.

(3) Miles, F. B. *J. Am. Chem. Soc.* **1968**, *90*, 1265.

(4) Krimse, W. W.; Streu, J. *J. Org. Chem.* **1985**, *50*, 4187.

(5) Sieber, S.; Schleyer, P. von R.; Vanik, H.; Mesi, M.; Sunko, D. E. *Angew. Chem. Int., Ed. Engl.* **1993**, *32*, 1604.

(6) Moss, R. A.; Fu, X. X.; Sauers, R. H. *Can. J. Chem.* **2005**, *83*, 1228.

(7) Bader, R. F. W. *Atoms in Molecules − A Quantum Theory*; Oxford University Press: Oxford, U.K., 1990.

(8) Werstiuk, N. H.; Muchall, H. M. *J. Mol. Struct. (THEOCHEM)* **1999**, *463*, 225.

(9) Werstiuk, N. H.; Muchall, H. *J. Phys. Chem. A* **1999**, *103*, 6599.

(10) Werstiuk, N. H.; Muchall, H. *J. Phys. Chem. A* **2000**, *104*, 2054.

(11) Werstiuk, H. H.; Muchall, H. M.; Noury, S. J. *Phys. Chem. A* **2000**, *104*, 11601.

(12) Bajorek, T.; Werstiuk, N. H. *Can. J. Chem*. **2005**, *83*, 1352.

(13) Poulsen, D. A.; Werstiuk, N. H. J. *Chem. Theory Comput.* **2006**, *2*, 77.

(14) Carlier, P. R.; Deora, N.; Crawford, T. D. *J. Org. Chem.* **2005**, *71*, 1592.

(15) Frisch, M. J.; Trucks, G. W.; Schlegel, H. B.; Scuseria, G. E.; Robb, M. A.; Cheeseman, J. R.; Montgomery, J. A., Jr.; Vreven, T.; Kudin, K. N.; Burant, J. C.; Millam, J. M.; Iyengar, S. S.; Tomasi, J.; Barone, V.; Mennucci, B.; Cossi, M.; Scalmani, G.; Rega, N.; Petersson, G. A.; Nakatsuji, H.; Hada, M.; Ehara, M.; Toyota, K.; Fukuda, R.; Hasegawa, J.; Ishida, M.; Nakajima, T.; Honda, Y.; Kitao, O.; Nakai, H.; Klene, M.; Li, X.; Knox, J. E.; Hratchian, H. P.; Cross, J. B.; Bakken, V.; Adamo, C.; Jaramillo, J.; Gomperts, R.; Stratmann, R. E.; Yazyev, O.; Austin, A. J.; Cammi, R.; Pomelli, C.; Ochterski, J. W.; Ayala, P. Y.; Morokuma, K.; Voth, G. A.; Salvador, P.; Dannenberg, J. J.; Zakrzewski, V. G.; Dapprich, S.; Daniels, A. D.; Strain, M. C.; Farkas, O.; Malick, D. K.; Rabuck, A. D.; Raghavachari, K.; Foresman, J. B.; Ortiz, J. V.; Cui, Q.; Baboul, A. G.; Clifford, S.; Cioslowski, J.; Stefanov, B. B.; Liu, G.; Liashenko, A.; Piskorz, P.; Komaromi, I.; Martin, R. L.; Fox, D. J.; Keith, T.; Al-Laham, M. A.; Peng, C. Y.; Nanayakkara, A.; Challacombe, M.; Gill, P. M. W.; Johnson, B.; Chen, W.; Wong, M. W.; Gonzalez, C.; Pople, J. A., Jr. *Gaussian 03, Revision B.02 and C.02*; Gaussian, Inc.: Wallingford, CT, 2004.

(16) Dennington, R., II; Keith, T.; Millam, J.; Eppinnett, K.; Hovell, W. L.; Gilliland, R. *GaussView, Version 3.09*; Semichem, Inc.: Shawnee Mission, KS, 2003.

(17) Biegler-Konig, F. *AIM 2000*; Copyright 1998−2000, University of Applied Science: Bielefeld, Germany.

(18) Keith, T. A. *AIMALL97 Package (D2) for WINDOWS.* aim@tkgristmill.com (accessed September 7, 2007).

(19) Wang, Y.-G.; Matta, C.; Werstiuk, N. H. *J. Comput. Chem.* **2003**, *24*, 1720.

(20) Wang, Y.-G.; Werstiuk, N. H. *J. Comput. Chem*. **2003**, *24*, 379.

(21) *NABLA. Fortran Program for computing the density and Laplacian of the density on a 3D grid using G94, G98, and G03 wave functions*; Dr. Stephane Noury, Department of Chemistry, McMaster University: 2000.

(22) IBM(1999). *Open Visualization Data Explorer*. Available: http://www.research.ibm.com/dx/ (accessed September 7, 2007).

(23) *ChemCraft, Version 1.5*. http://www.chemcraftprog.com.

(24) Xantheas, X. S. X. S.; Elbert, T. S. T. S.; Ruedenberg, K. *Theor. Chim. Acta* **1991**, *78*, 365.

(25) Pendás, A. M.; Francisco, E.; Blanco, M. A.; Gatti, C. *Chem. Eur. J.* **2007**, DOI: 10.1002/chem.200700408.

(26) Farrugia, L. J.; Evans, C.; Tegel, M. *J. Phys. Chem. A* **2006**, *110*, 7952.

(27) Sunko, D. E.; Vančik, H.; Mihalić, Z.; Shiner, V. J.; Wigles, F. P. *J. Org. Chem.* **1994**, *59*, 7051.

CT700176D